Supporting Information

Selectively "Size-Excluding" Water Molecules to Enable Highly Reversible Zinc Metal Anode

Xiaowei Shen[a,†], Wanhao Chen[b,c,†], Haocong Wang[e], Lifang Zhang[b], Baojiu Hao[b], Changhao Zhu[b], Xiuzhen Yang[b], Meizhu Sun[b], Jinqiu Zhou[b,*], Xuejun Liu[c,*], Chenglin Yan[d,e], Tao Qian[b,*]

[a] School of Electrical Engineering, Nantong University, Nantong 226019, China

[b] School of Chemistry and Chemical Engineering, Nantong University, Nantong 226019, China

[c] College of Chemistry and Chemical Engineering, State Key Laboratory of Bio-fibers and Eco-textiles, Qingdao University, Qingdao 266071, China

[d] School of Petrochemical Engineering, Changzhou University, Changzhou 213164, China

[e] Key Laboratory of Core Technology of High Specific Energy Battery and Key Materials for Petroleum and Chemical Industry, College of Energy, Soochow University, Suzhou 215006, China

[†] The authors contributed equally to this work.

E-mails: jqiuzhou@ntu.edu.cn (J. Zhou); xjliu@qdu.edu.cn (X. Liu); qiantao@ntu.edu.cn (T. Qian).

Experimental Section

Materials. Commercial Zn foil (0.1 mm) and Cu foil (0.1 mm) were purchased from Ailian of Tianjin, Ltd. Copper nitrate trihydrate ($Cu(NO_3)_2 \cdot 3H_2O$, >99.0%), decanoic acid ($C_{10}H_{20}O_2$, >99.5%), octanoic acid ($C_8H_{16}O_2$, >99.5%), hexadecanoic acid ($C_{16}H_{32}O_2$, >99.5%), sodium hydroxide (NaOH, >97.0%), ethanol (C_2H_5OH, >99.0%), vanadium pentoxide (V_2O_5, >99.5%), zinc sulfate heptahydrate ($ZnSO_4 \cdot 7H_2O$, >99.0%), and sodium sulfate (Na_2SO_4, >99.0%) of analytic grade were purchased from the Aladdin and used as received without further purification.

Preparation of the metal soaps CuC_n. For CuC_9, 2.41 g $Cu(NO_3)_2 \cdot 3H_2O$ was dissolved in 10 mL deionized water. A mixture of 3.44 g decanoic acid and 0.8 g NaOH was also dissolved in 10 mL deionized water. Then the two solutions were mixed to get blue precipitate in a few seconds. In all cases, the precipitate was filtered and washed with water. The powder was obtained by drying in a spin evaporator to obtain the solid blue powder. Meanwhile, metal soap CuC_7 and CuC_{15} were prepared using octanoic acid and hexadecanoic acid using the same method.

Preparation of the Zn@CuC_n anode. The Zn@CuC_9 electrode was fabricated through an in electrospray self-assembly route. Firstly, we weighed 2g CuC_9, dissolved them in 20 mL of anhydrous ethanol and performed ultrasonication for 1 hour to prepare dispersion (The dispersity of CuC_9 in ethanol is better than in H_2O). The dispersion was put into an electric gun and sprayed onto the zinc foil with a certain sputtering time. The zinc foil was heated at 120 °C for 40 min, and then cooled down slowly to form the membranes. Meanwhile, Zn@CuC_7 and Zn@CuC_{15} were prepared by the same process.

Preparation of the NVO cathode material. Firstly, 1.819 g V_2O_5 and 0.400 g NaOH were dissolved in 40 mL deionized water under magnetically stirring for 30 min. After that, the solution was transferred to 50 mL autoclave and kept at 180 ℃ for 48 h. Then, the product in autoclave were collected by centrifugation and washed with deionized water and ethanol for 3 times, respectively, and dried at 80 ℃ in vacuum for 12 h. After heating at 300 ℃ in the air for 2 hours, the NVO powder was obtained.

Characterizations. The crystallographic phase of the as-prepared products was studied by X-ray power diffraction (XRD, Rigaku D/max2500). For analyzing pore structure, H_2O (298 K) and N_2 (77 K) sorption experiments were performed with ASAP 2460 (Micromeritics Corp., USA). The morphologies of the samples were characterized by scanning electron microscopy (Gemini SEM 300

(Japan)). Four-probe resistance results were obtained from tester H7756 and contact angle results were obtained from DSA 25 (KRUSS). The generation of H_2 was analyzed by gas chromatography (GC-2014, Shimadzu). Atomic force microscopy (AFM) and Kelvin probe force microscopy (KPFM) images were obtained using an Omega Scope 1000 system from AIST-NT. X-ray photoelectron spectroscopy (XPS) measurements were obtained on a spectrometer (Escalab 250xi, Thermo Scientific).

Electrochemical Measurements. Linear scanning voltammetry (LSV), Tafel plot, CV and Electrochemical Impedance Spectroscopy (EIS) tests are performed on a CHI760E electrochemical workstation. The LSV was tested using a Zn@CuC_9 batteries with a scan rate of 1 mV s^{-1}. The Tafel plot test used a three-electrode system (Working electrode: Zn, Counter electrode: Pt, Reference electrode: Ag/AgCl, Salt bridge: Saturated KCl solution) with a scan rate of 1 mV s^{-1}. The electrochemical performances of Zn//Zn or Zn//Cu half batteries, and Zn//NVO full batteries were tested in the form of encapsulated coin batteries (CR2032). Glass fiber separators (GF/A) were used in all coin cells. Testing of batteries for galvanostatic charge/discharge cycles is performed on the Neware battery testing system. The Zn//Zn symmetric batteries were cycled with different current densities and capacities. The Zn//Cu batteries were cycled with a fixed discharge capacity and charge cut-off voltage of 1 V. For full Zn//NVO batteries, NVO cathode loading is 1-2 mg cm^{-2}. The scan rate for CV testing of Zn//NVO full batteries is 1 mV s^{-1}. Zn//NVO full batteries were cycled in the voltage range of 0.4-1.4 V.

DFT calculations. One units CuC_n was used to stand for the system of CuC_n to simulate the behavior of Zn^{2+} and H_2O in different carbon chain. All DFT calculations were performed on Vienna ab initio simulation package (VASP). The generalized gradient approximation (GGA) within the framework of Perdew-Burke-Ernzerhof (PBE) functional was used for the description of exchange-correlation potential. The van der Waals (vdW) interaction was considered using the zero damping DFT-D3 method of Grimme. An energy cutoff of 450 eV and Γ k-point sampling sets of 1 × 1 × 1was used to be converged. The criterion for all structural optimizations was set to 10^{-5} eV for electronic energy convergence and Hellmann-Feynman force less than 0.02 eV/Å for ionic relaxation loop. The implicit solvent model, VASPsol, was applied to considered effects between the solute and solvent in all DFT simulations energies.

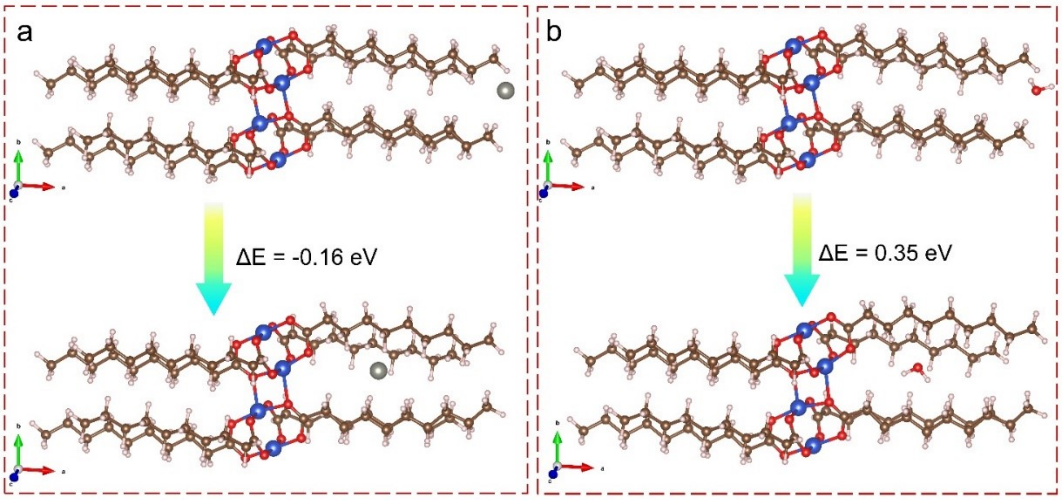

Figure S1. The calculated energy difference of (a) zinc ions and (b) water molecule into the channel between decyl group chains of CuC_9.

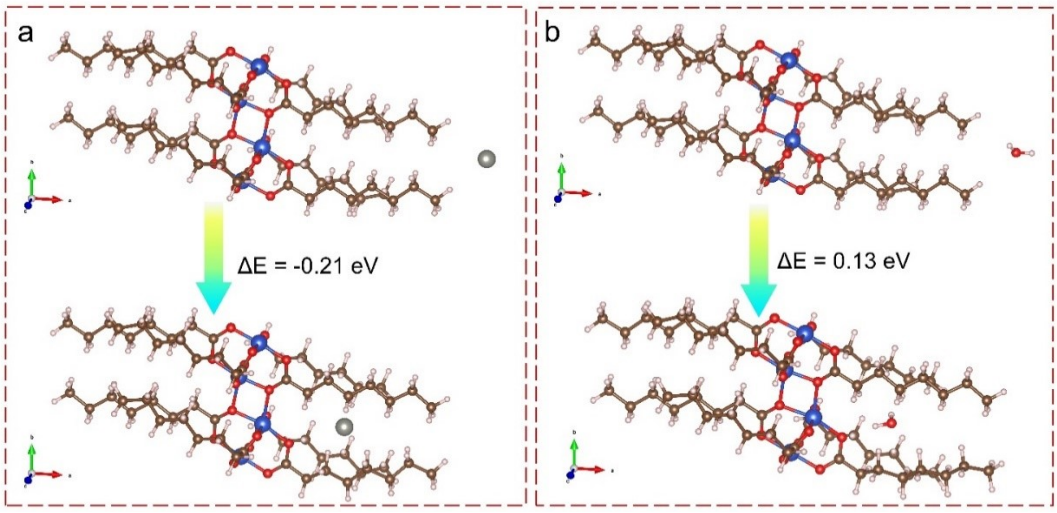

Figure S2. The calculated energy difference of (a) zinc ions and (b) water molecule into the channel between octyl group chains of CuC_7.

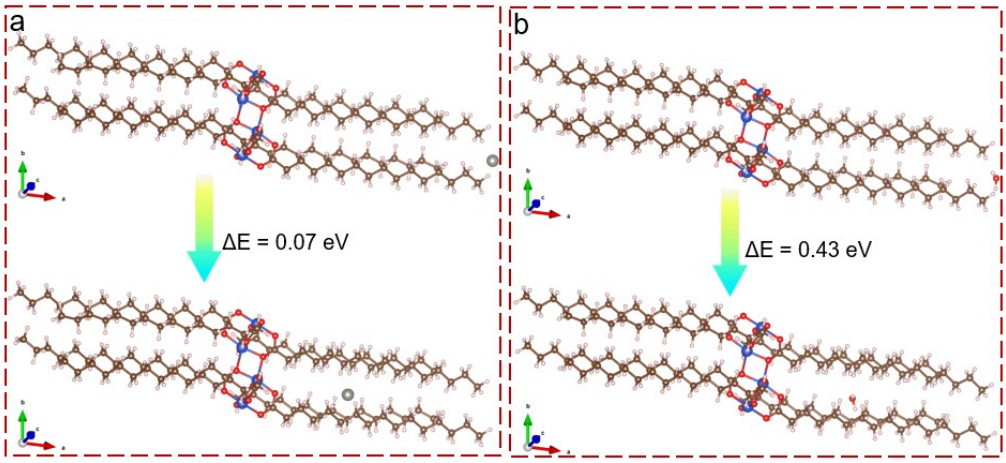

Figure S3. The calculated energy difference of (a) zinc ions and (b) water molecule into the channel between cetyl group chains of CuC_{15}.

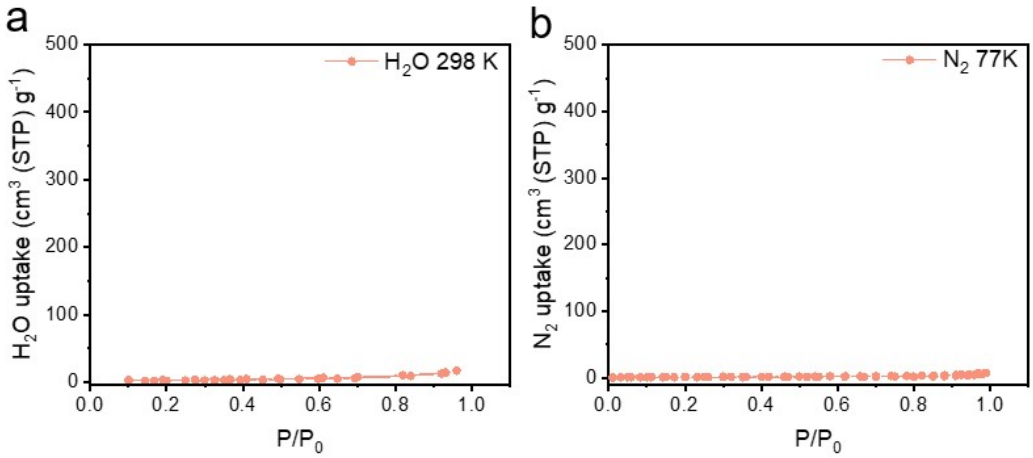

Figure S4. (a) H_2O adsorption isotherms of CuC_9 at 298 K; (b) N_2 adsorption isotherms of CuC_9 at 77 K.

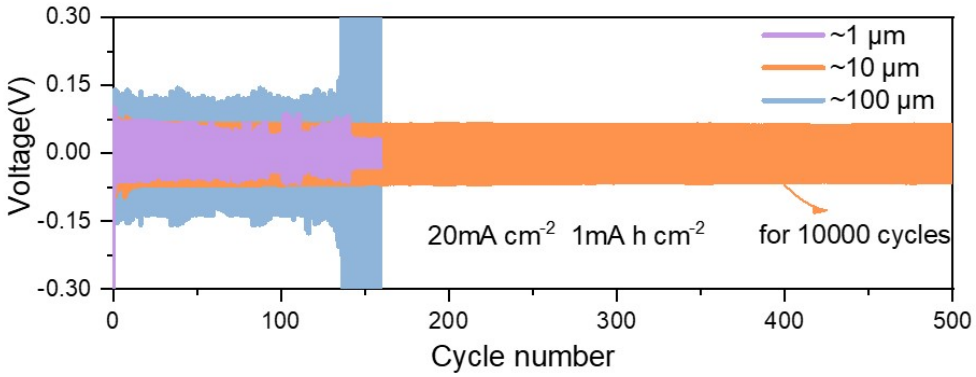

Figure S5. Symmetric cells of Zn@CuC_9 with different thickness of Cu soap films at 20 mA cm^{-2}-1 mAh cm^{-2}.

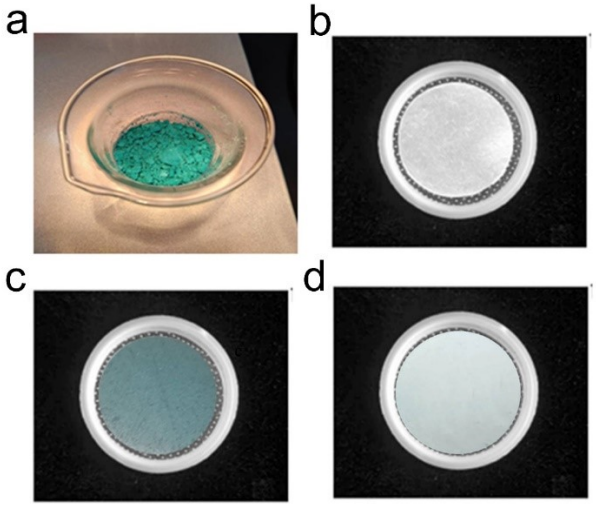

Figure S6. (a) A digital photo of the metal soap (CuC_9). The optical pictures of (b) the bare Zn, Zn@CuC_9 anode (c) before and (d) after heating.

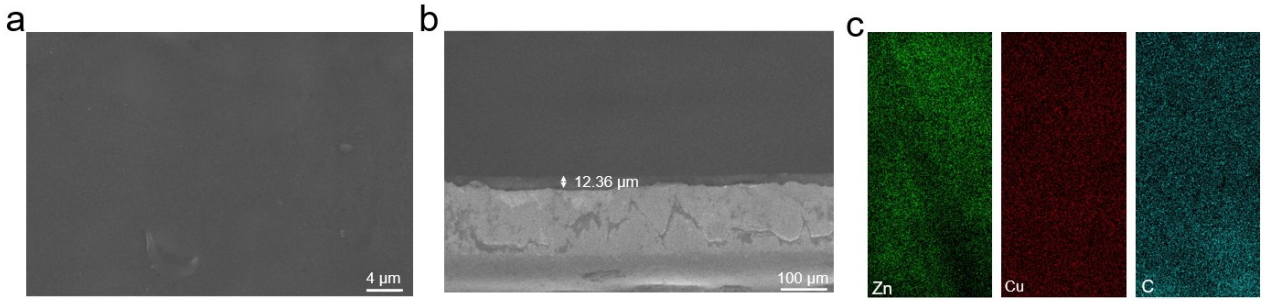

Figure S7. (a) top-view, (b) cross-sectional SEM images, and (c) corresponding EDS mapping of as-synthesized Zn@CuC_9 before cycling.

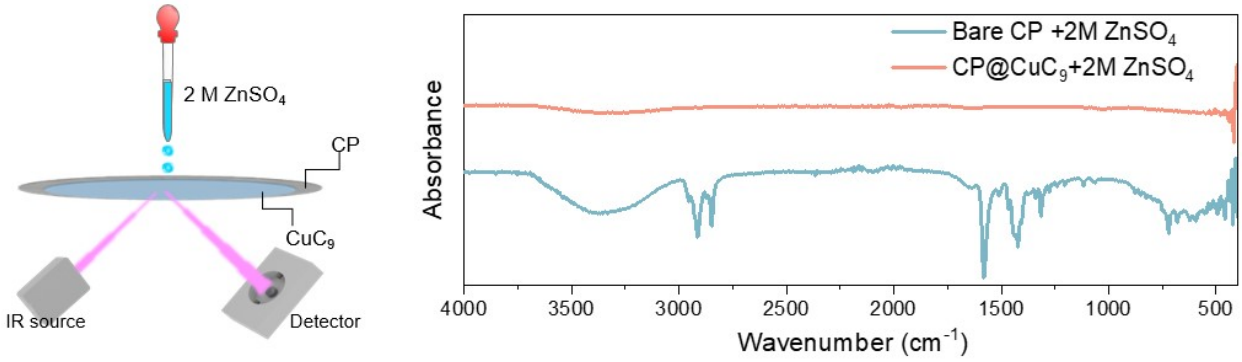

Figure S8. FTIR spectra of "Bare CP+2 M $ZnSO_4$" and "CP@CuC_9+2 M $ZnSO_4$".

Hydrophilic carbon paper (CP) is used as substrate of zinc salt (2 M $ZnSO_4$) solution to determine the free-water molecules. A metal soap film is attached to one side of CP to prepare CP@CuC_9. As shown in Figure S8, the FTIR spectra of "Bare CP+2 M $ZnSO_4$" and "CP@CuC_9+2 M $ZnSO_4$" are tested to determine the penetration of free water into CuC_9 film. As a reference, free-water molecules give rise to a broad band of O-H stretching vibration located at ≈ 3370 cm^{-1} owing to the H-bonding environments of water clusters.[S1] It is found that almost no identifiable peaks associated with free water molecules are detected in the vicinity of 3370 cm^{-1} (O-H stretching), which is a strong evidence that the CuC_9 film contains virtually no free water molecules.

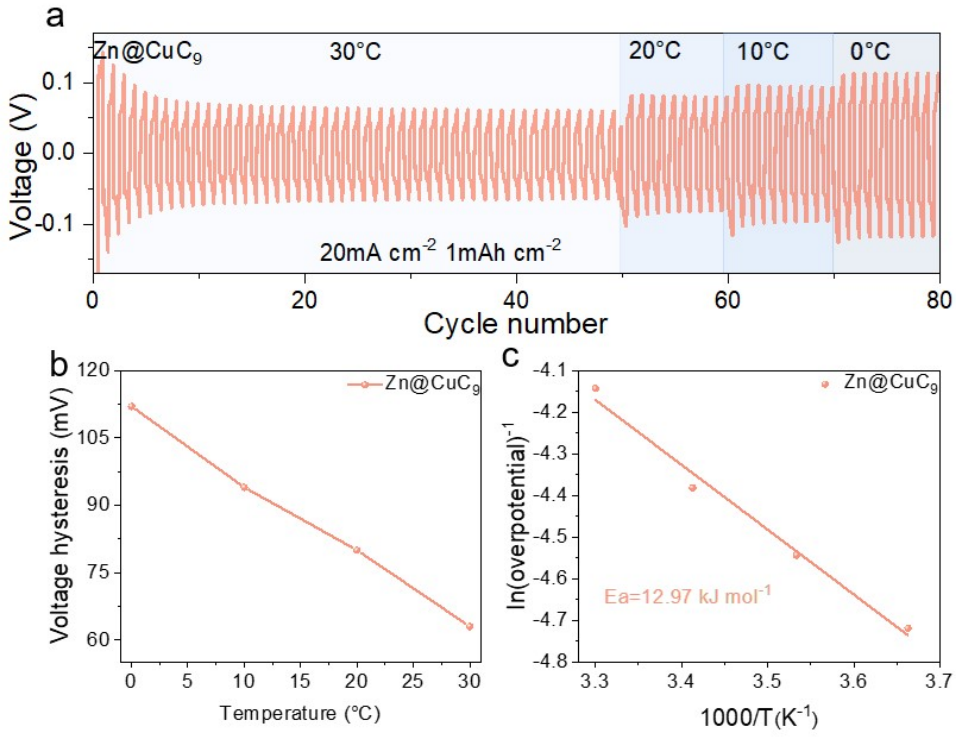

Figure S9. (a) Symmetrical cells of $Zn@CuC_9$ at different temperatures. (b) summarized overpotentials of the cells under various temperatures; (c) corresponding activation energies of the reaction.

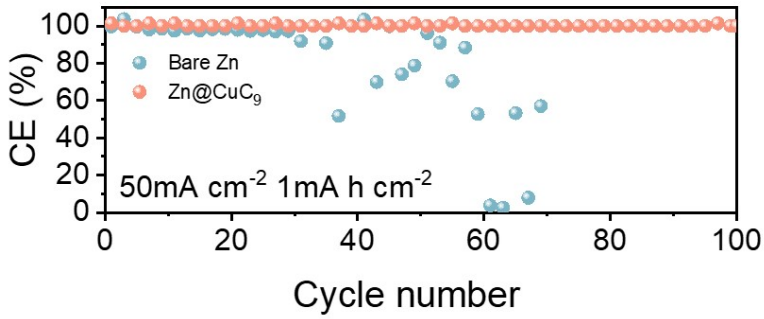

Figure S10. CE of the asymmetric Zn//Cu half-cells with and without CuC_9 interface at 50 mA cm^{-2}, 1 mA h cm^{-2}.

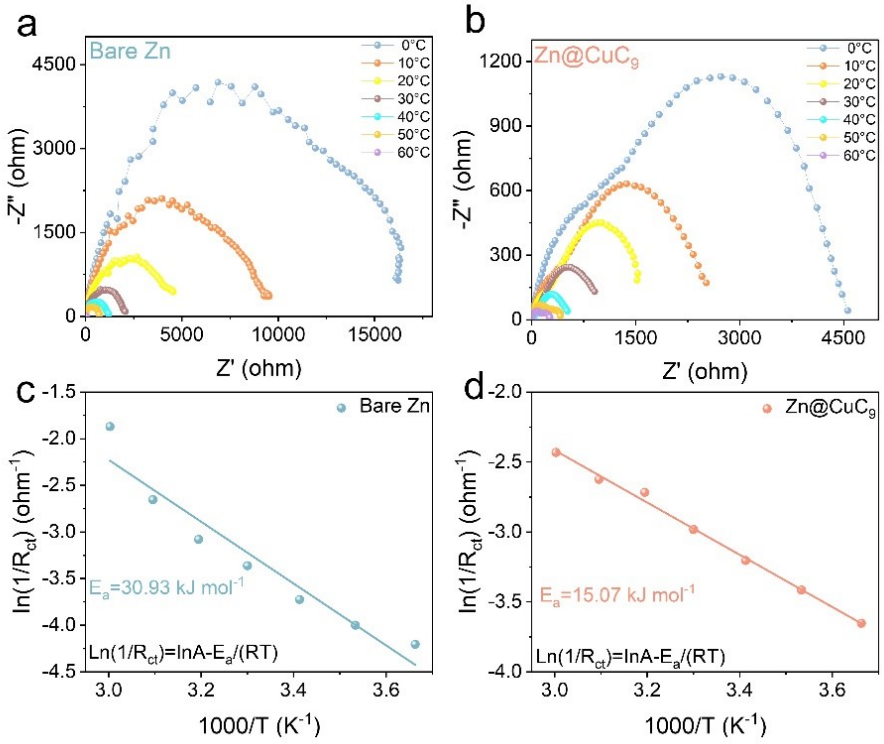

Figure S11. (a-b) EIS results at different temperatures. (c-d) Arrhenius curve comparison.

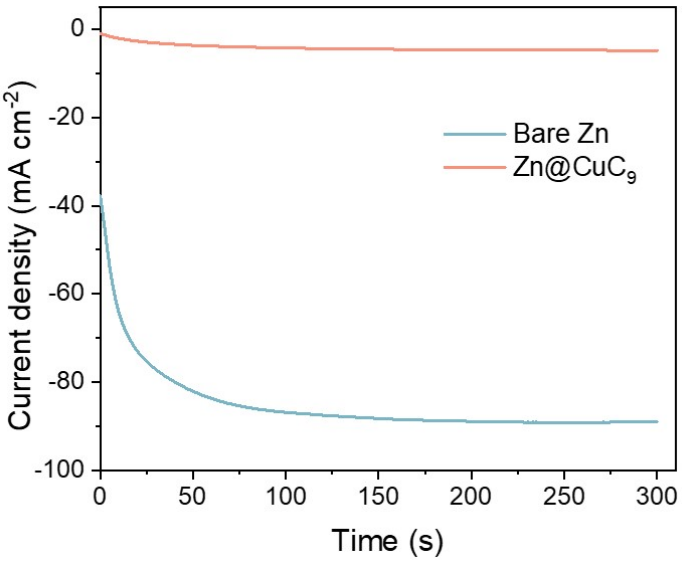

Figure S12. CA profiles of Zn//Zn symmetric cells with and without Cu soap film under a voltage of -150 mV.

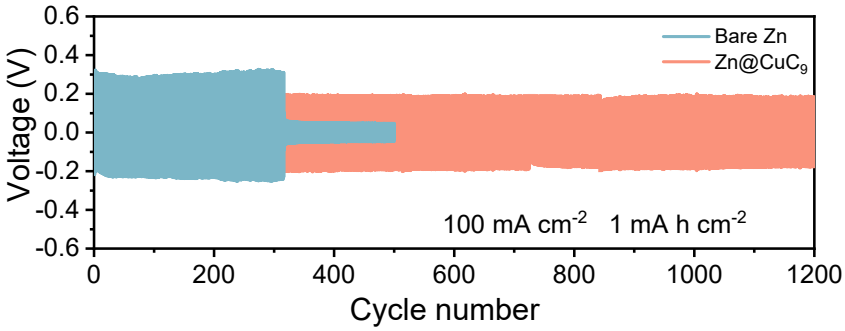

Figure S13. Cycling reversibility test of symmetric cells with bare Zn or Zn@CuC_9 electrode under current densities 100 mA cm^{-2} with 1 mA h cm^{-2}.

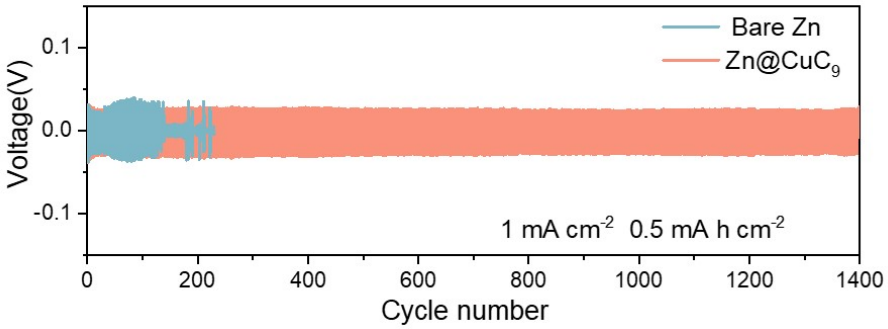

Figure S14. Symmetric half-cells of bare Zn and Zn@CuC_9 at 1 mA cm^{-2}-0.5 mA h cm^{-2}.

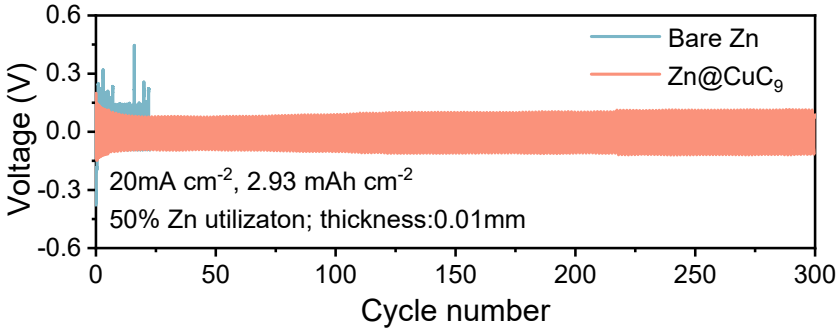

Figure S15. Performance of Symmetric Zn//Zn half-cells with 50% utilization rate by using ultrathin Zn foil (thickness of 0.01mm).

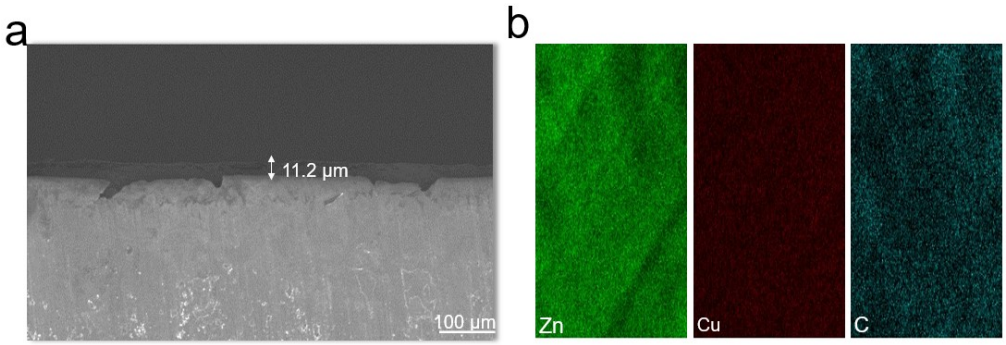

Figure S16. (a) cross-sectional SEM images, and (b) corresponding EDS mapping of Zn@CuC_9 after cycling.

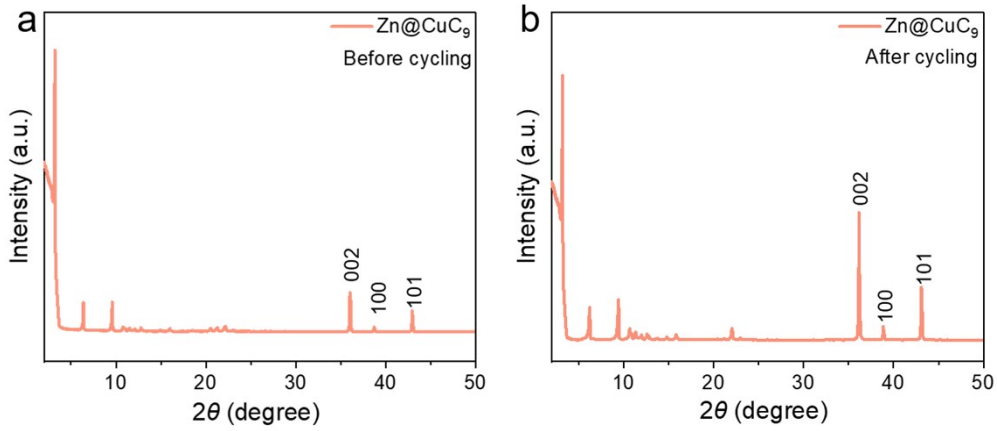

Figure S17. XRD spectra of the Zn@CuC_9 anodes before and after cycling.

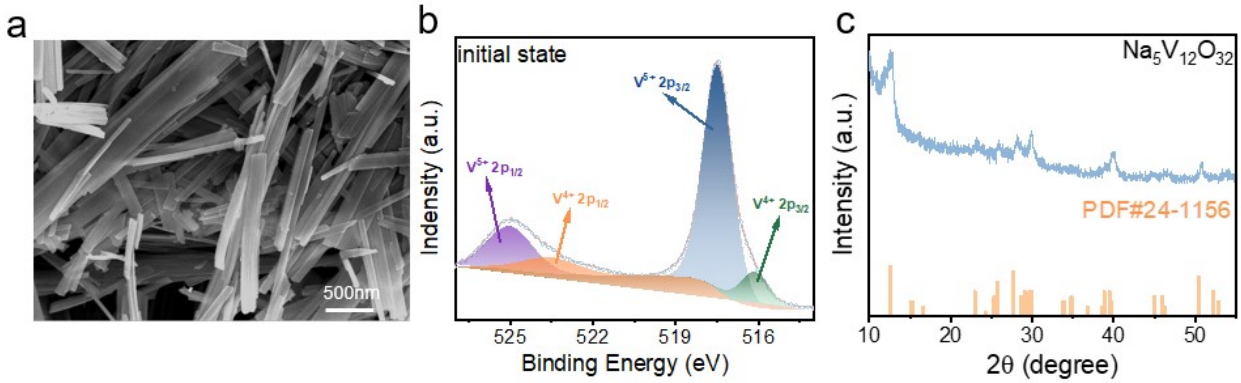

Figure S18. Characterization of the synthesized NVO: (a) SEM, (b)XPS, (c) XRD.

The morphology and phase of the synthesized NVO powder have been characterized by SEM, XPS and XRD. NVO displays nanobelt morphology (Figure S18a), typically with a length of several micrometers and a width of about 200 nm. As shown in Figure S18b, the V $2p_{3/2}$ peak at initial state can be divided into two different peaks located at 516.7 and 517.4 eV, which correspond to V^{4+} $2p_{3/2}$ and V^{5+} $2p_{3/2}$, respectively. All the diffraction peaks of NVO match well with the monoclinic NVO phase (Figure S18c).[66]

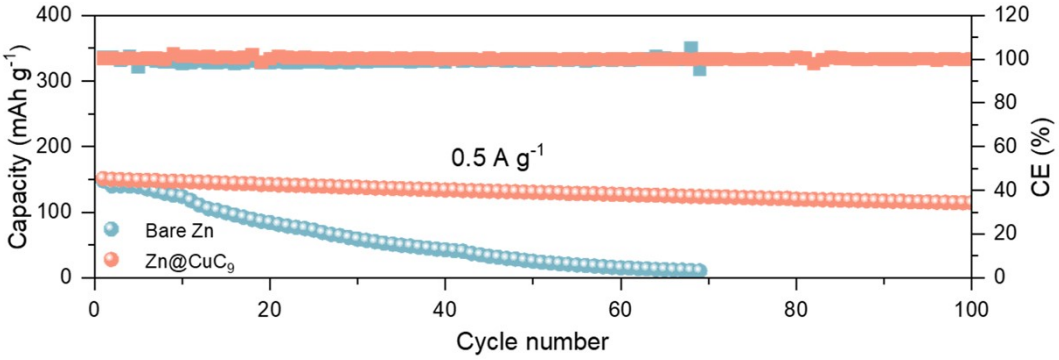

Figure S19. Cycling stability of bare Zn//NVO and Zn@CuC_9//NVO full cells at a low rate of 0.5 A g^{-1}.

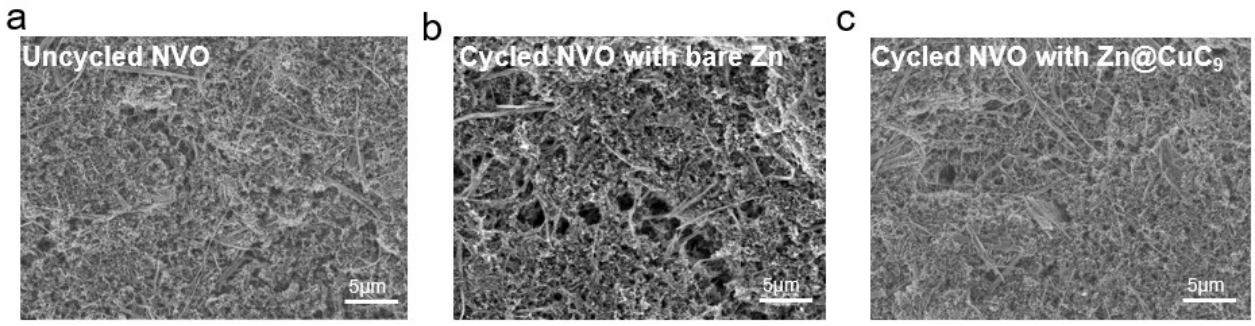

Figure S20. The SEM of (a) uncycled NVO, (b) cycled NVO with bare Zn, and (c) cycled NVO with Zn@CuC_9.

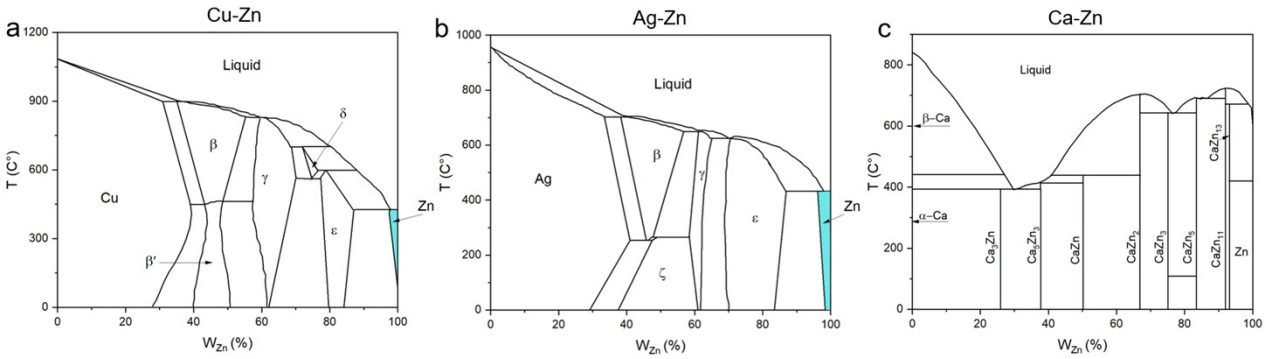

Figure S21. The binary phase diagram of the (a) Cu-Zn system, (b) Ag-Zn system and (c) Ca-Zn system.

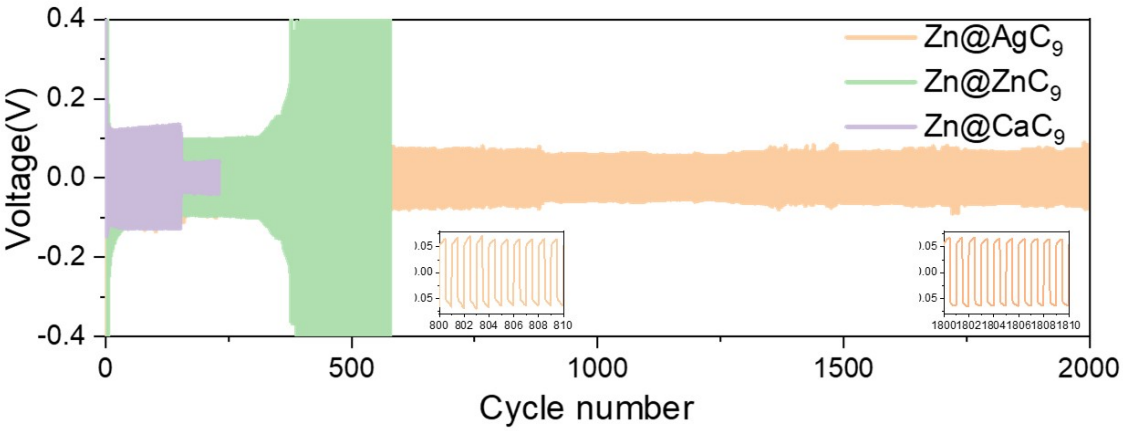

Figure S22. Symmetric cells of $Zn@CaC_9$, $Zn@ZnC_9$ and $Zn@AgC_9$ at 20 mA cm^{-2}-1 mA h cm^{-2}.

Table S1. Crystal data of different metal soaps.

Crystal data	**CuC_7**	**CuC_9**	**CuC_{15}**
space group	P-1 (2)	*C2/c* (15)	*C2/c* (15)
a (Å)	5.14137	55.68300	85.15700
b (Å)	8.51928	5.10660	5.05300
c (Å)	22.12405	16.50200	16.10600
α (°)	83.773	90	90
β (°)	84.562	93.93	91.288
γ (°)	76.144	90	90

Table S2. H_2 production rate of different sampling times.

Sample	H_2 production rate (μg h^{-1})				
	6^{th} min	12^{th} min	18^{th} min	24^{th} min	30^{th} min
Bare Zn	1.41	1.52	1.65	1.70	1.78
Zn@CuC_9	0.02	0.12	0.12	0.13	0.13

References

S1 T. Liu, X. Du, H. Wu, Y. Ren, J. Wang, H. Wang, Z. Chen, J. Zhao, and G. Cui, *Angew. Chem. Int. Ed.*, 2023, **62**, e202311589.